Biochimica et Biophysica Acta 1808 (2011) 140–153

Contents lists available at ScienceDirect

Biochimica et Biophysica Acta

journal homepage: www.elsevier.com/locate/bbamem

The vesicle-to-micelle transformation of phospholipid–cholate mixed aggregates: A state of the art analysis including membrane curvature effects

Mustafa M.A. Elsayed [a], Gregor Cevc [b,*]

[a] IDEA AG, Frankfurter Ring 193a, 80807 Munich, Germany
[b] Advanced Treatments Institute, Tassilostr. 3, 82131, Gauting, Germany

ARTICLE INFO

Article history:
Received 22 April 2010
Received in revised form 5 August 2010
Accepted 1 September 2010
Available online 9 September 2010

Keywords:
Cholate
Phosphatidylcholine
Lipid solubilisation
Bilayer curvature
Aggregate size
Static light scattering
Dynamic light scattering

ABSTRACT

We revisited the vesicle-to-micelle transformation in phosphatidylcholine–cholate mixtures paying special attention to the lipid bilayer curvature effects. For this purpose, we prepared unilamellar vesicles with different starting sizes ($2r_v$ = 45–120 nm). We then studied mixtures of the unilamellar vesicles (1–8 mmol kg^{-1}) and sodium cholate (0–11.75 mmol kg^{-1}) by static and dynamic light scattering. The transformation generally comprises at least two, largely parallel phenomena; one increases and the other decreases the average mixed aggregate size. In our view, cholate first induces bilayer fluctuations that lead to vesicle asphericity, and then to lipid bilayer poration followed by sealing/reformation (or fusion). The cholate-containing mixed bilayers, whether in vesicular or open form, project thread-like protrusions with surfactant enriched ends even before complete bilayer solubilisation. Increasing cholate concentration promotes detachment of such protrusions (i.e. mixed micelles formation), in parallel to further softening/destabilising of mixed amphipat bilayers over a broad range of concentrations. Vesicles ultimately fragment into mixed thread-like micelles. Higher cholate relative concentrations yield shorter thread-like mixed micelles. Most noteworthy, the cholate-induced bilayer fluctuations, the propensity for large aggregate formation, the transformation kinetics, and the cholate concentration ensuring complete lipid solubilisation all depend on the starting mean vesicle size. The smallest tested vesicles ($2r_v$ = 45 nm), with the highest bilayer curvature, require ~30% less cholate for complete solubilisation than the largest tested vesicles ($2r_v$ = 120 nm).

1. Introduction

Bile salts are a special group of physiological detergents, or biosurfactants, with a major role in lipid absorption in the intestine. The chemical structure of bile salts differs from that of typical head–tail surfactants (e.g. alkyl glucosides, alkyl sulphates, fatty acid polysorbates), which consist of a polar "head" with one or several hydrophilic groups attached to a separate hydrophobic chain/s, or a "tail". In contrast, each bile salt molecule has a rigid steroid core with one lipophilic, convex surface and one hydrophilic, polyhydroxylated, concave surface [1] (Fig. 1). The ring system is central in bile salt interactions with other molecules. The self- and hetero (with various lipids)-aggregation of bile salts and head–tail surfactants therefore differ in detail.

Bile salt–lipid interactions are of physiological and fundamental interest. They are a key to understanding intestinal fat digestion and absorption [2] and the basis for various applications. In biochemistry, for example, bile salts are used to isolate membrane proteins and to reconstitute such proteins into lipid bilayers [3–6]. In pharmaceutics, bile salts are included into some drug delivery systems, such as mixed micelles [7] (e.g. Konakion® MM, Valium® MM) or ultradeformable mixed lipid vesicles [8–16]. The self-assembly, i.e. the homo-aggregation, of bile salts into micelles and their hetero-aggregation with other lipids that tend to form bilayers, such as the ubiquitous phosphatidylcholines, are of physicochemical significance as well.

Phospholipid–bile salt mixtures were extensively investigated for decades, with a special early focus on lipid/cholesterol solubilisation and a later focus on vesicle-to-micelle transformation [1–3,5,17–31]. A large body of experimental data was thus collected over the years, but some important questions remain open. To our knowledge, the mixed aggregates detailed morphology and molecular composition, and especially their interrelationship in the transition region, are not yet fully elucidated. Trying to avoid repetition, we tackle herein these questions only to the extent necessary to understand the whole picture. In contrast, we pay full attention to the previously neglected curvature effects on bilayer solubilisation and on to the comparability of vesicle-to-micelle with micelle-to-vesicle transformation. Unlike previous researchers in the field we also ensure complete cholate ionisation during the process, as cholate like other ionic surfactants is (maximally) active only in its ionised form.

In this report we address the complete sequence of structural and morphological changes occurring during the vesicle-to-micelle

* Corresponding author. Tel.: +49 89 89 355 771; fax: +49 89 903 65 07.
E-mail addresses: mmaelsayed@gmail.com (M.M.A. Elsayed), cevc@advanced-treatments.org (G. Cevc).

0005-2736/$ – see front matter © 2010 Published by Elsevier B.V.
doi:10.1016/j.bbamem.2010.09.002

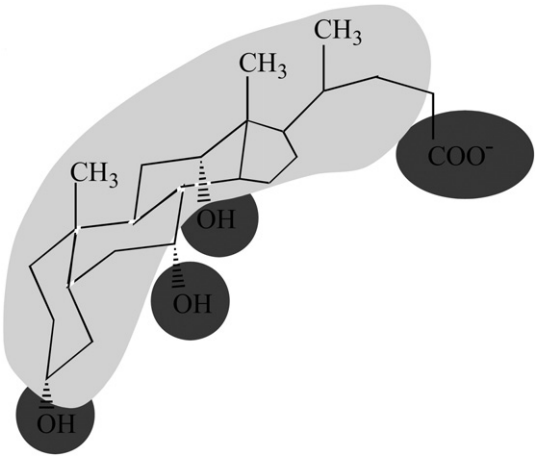

Fig. 1. The structural and chemical formula of a cholate molecule, showing the hydrophobic surface (light grey) and the hydrophilic groups (dark grey) on the other molecular side (modified from [1]).

transformation in phosphatidylcholine–sodium cholate mixtures under consideration of (local) bilayer curvature effects and with special focus on the presolubilisation region. For this purpose, we studied the initial vesicle size effects on natural phosphatidylcholine vesicle transformation into the cholate dominated mixed micelles, relying on static and dynamic light scattering data. We analysed the results with several theoretical models to explain experimental observations more quantitatively, and paid some attention to the studied process kinetics as well. The emerging picture of vesicle-to-micelle transformation is richer but also more complex than previously known, which raises some experimental caveats. To list but the most important ones: the very popular optically measured "bilayer-saturating concentration" is an ill-defined "descriptor" with an assay-, preparation history-, and size-dependent value; the "three-step solubilisation" model is pedagogically useful but never strictly applicable to reality, where continuous solubilisation prevails; the bilayer solubilising concentration is the only robust descriptor of lipid solubilisation in the tested mixtures, but it also depends on the starting aggregate size and is potentially burdened with the slow transition kinetics; the results measured with only partially ionised surfactant molecules are questionable due to interfacial effects on molecular charge, and vice versa. Arguably, these caveats apply to most, if not all, lipid–surfactant mixtures.

2. Materials and methods

2.1. Materials

We obtained soybean phosphatidylcholine (SPC, Lipoid S 100, purity = 97.8%, the assumed average molecular weight ~800 g/mol) from Lipoid GmbH (Ludwigshafen, Germany). Sodium cholate hydrate (purity ≥ 97%) was from Sigma-Aldrich (Steinheim, Germany). All the other chemicals and reagents were of analytical grade. Polycarbonate membranes were from GE Water & Process Technologies (Trevose, PA, U.S.A.).

2.2. Preparation of lipid vesicles

In brief, we dissolved the necessary amount of phosphatidylcholine in a sufficient amount of chloroform in a 500 mL round-bottom flask. We evaporated the solvent under vacuum at 50 °C in a rotary evaporator. This yielded a thin lipid film, which we hydrated at the same temperature with bidistilled water. The ensuing suspension of multilamellar vesicles (MLV) had a total phospholipid concentration of 120 mg g^{-1} (~150 mmol kg^{-1}). We then produced large unilamellar vesicles (LUV) from such MLV by extruding the original "crude" suspension 10 times through a set of polycarbonate membranes with 80 nm pores under 1.75 MPa (254 psi) nitrogen gas pressure. To gain intermediate-size unilamellar vesicles (IUV), we further extruded the LUV suspension eight times through a set of polycarbonate membranes with 30 nm pores under nitrogen gas pressure of 2.50 MPa (= 363 psi). To obtain the smallest achievable unilamellar vesicles (SUV), we sonicated the IUV suspension on ice with a Sonopuls HD 3100 ultrasonic probe homogenizer (Bandelin electronic, Berlin, Germany) until the suspension became opalescent (using an MS 73 tip and a sonication power of 20 W, this took approximately 150 min for a 25 g sample). Finally, we filtered the sonicated SUV suspensions through a polycarbonate membrane with 80 nm pores under 1.75 MPa nitrogen gas pressure to remove the titanium particles originating from the ultrasound transducing tip. We measured the final phospholipid concentration with HPLC to confirm that no lipid material was lost during preparation. For this purpose, we used an in-house modification of the method described by Nasner and Kraus [32], with refractive index detection [33].

2.3. Preparation of samples

We prepared vesicle suspensions with different lipid concentrations in an aqueous carbonate buffer (50 mM, pH = 10.25) adjusted with NaCl to a final ionic strength of 150 mM. For this purpose, we diluted the original LUV, IUV, or SUV suspensions, prepared in distilled water, with appropriate volumes of the buffer. We always prepared fresh samples immediately before starting an experiment to minimise lipid degradation/hydrolysis at the high chosen pH. We also prepared a series of sodium cholate solutions/suspensions with different concentrations in a similar buffer, and adjusted each preparation to 150 mM ionic strength with NaCl. We then mixed an aliquot of the tested vesicle suspension with an equal volume of the appropriate sodium cholate solution/suspension by stirring the blend thoroughly. For the steady state experiments, we left each mixture to equilibrate at room temperature (~25 °C), until its optical density became constant. We then recorded the static and the dynamic light scattering data of each separately prepared mixture. To conduct the time-resolved measurements, we mixed the individual components in a jacketed (25 °C) glass reservoir connected to a flow-through quartz cuvette with peristaltic pump tubing. An eight-channel Gilson (Villiers le Bel, France) Minipuls-3 peristaltic pump maintained a steady suspension flow through the cuvette, in which we recorded the optical density continuously until reaching a constant value. To assess phosphatidylcholine hydrolysis during experiments, we checked phosphatidylcholine and lysophosphatidylcholine concentrations in representative samples with the described HPLC method.

2.4. The static light scattering (turbidimetry)

We measured the static light scattering (optical density) with a Shimadzu UV-1601 double-beam UV–VIS spectrophotometer equipped with a 6 position, automated sample changer and the Shimadzu UVProbe version 2.0 software (Shimadzu Corporation, Kyoto, Japan). We first confirmed that the light absorbed by SPC in the employed concentration range is negligible between 400 nm and 500 nm. We then read the optical density of the tested LUV and IUV mixtures at 500 nm. For the SUV mixtures we recorded the optical density at 400 nm to increase sensitivity and then properly allowed for the difference in the final data analysis.

2.5. The dynamic light scattering (photon correlation spectroscopy)

We used an ALV-NIBS/HPPS particle sizer (ALV-Laser *Vertriebsgesellschaft mbH*, Langen, Germany) for the dynamic light scattering measurements. We characterised each sample at 25 °C in three

individual measurements and then analysed the results with the ALV-5000/E/EPP software (version 3.0, regularised fit routine) based on the CONTIN 2DP method [34,35]. In so doing, we also accounted for temperature, salt and cholate effects on the dispersion medium viscosity. In brief, we started with the dynamic viscosity of water at 25 °C, being 0.89038 cP [36]. We then calculated the dynamic viscosity of the employed aqueous carbonate buffer following Pereira et al. [36] to be 0.91711 cP. We subsequently allowed for sodium cholate effects on the dispersion medium viscosity, relying on the data of Wang and colleagues [37] (lacking any reliable information on cholate binding under our experimental conditions, we assumed for this purpose that all cholate molecules are dissolved in the aqueous medium; this overestimates rather than underestimates the surfactant effects). This revealed that sodium cholate in the investigated concentration range affects the dispersion medium viscosity, and thus our analytical results, only little (<3%). For better accuracy we nonetheless included the correction in our analyses. Allowance for cholate binding effect would introduce only a practically negligible correction.

2.6. Data analysis

We analysed all experimental data either with Microcal Origin (version 6.0, Microcal Software, Inc., Northampton, MA, USA) or with a suitable Mathcad (version 11.0b, Mathsoft Engineering & Education, Inc., Cambridge, MA, USA) programme.

3. Results

To explore bilayer curvature effects on phospholipid–cholate interactions and bilayer solubilisation we first prepared essentially unilamellar soybean phosphatidylcholine bilayer vesicles with the different sizes summarised in Table 1.

3.1. The quasi-steady state light scattering

3.1.1. Large unilamellar vesicles (LUV)

Large unilamellar vesicles (LUV) change their optical density promptly after addition of sodium cholate, but ultimately attain a constant optical density. The upper panel in Fig. 2 shows such final constant molar optical density value as a function of total phospholipid and total cholate concentrations. The lower panel gives the corresponding mean diameter of the mixed aggregates as determined with the dynamic light scattering. The figure also contains information on the intensity-normalised fraction of the peak pertaining to the mixed lipid vesicles and/or to other large mixed aggregates in each preparation.

As is evident from Fig. 2, increasing total cholate concentration alters optical density of the studied suspensions non-monotonously. The initial optical density change is negative and relatively sharp (around −30% per mmol total cholate kg^{-1}). The change then turns positive, with a flatter slope, and finally becomes negative again. The final slope is steep in the first part and flatter towards the end of each solubilisation curve. Lipid concentration can enhance or suppress this sequence of changes and slopes.

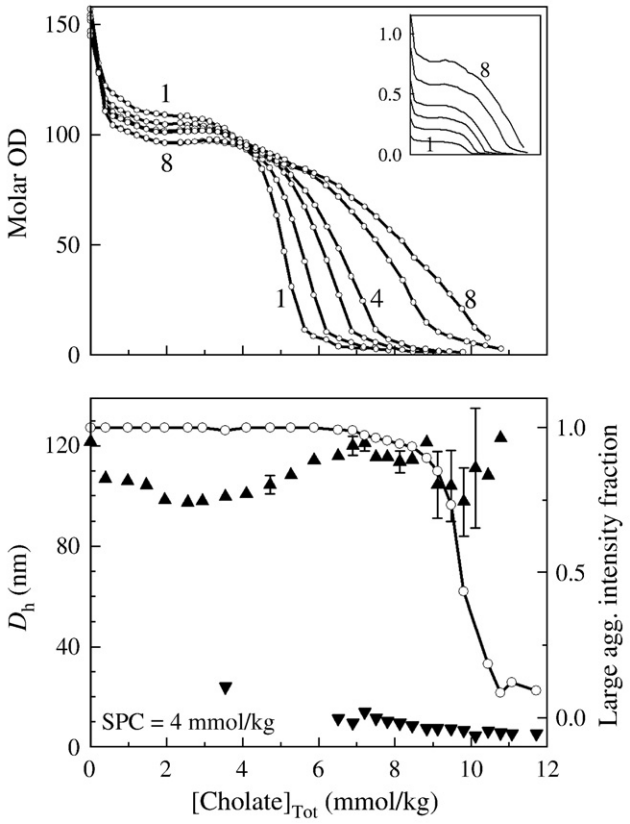

Fig. 2. Upper panel: The molar optical density (quasi-steady state, λ = 500 nm) of the mixed aggregate suspension resulting from the LUV after addition of sodium cholate to the given total concentration. The numbers next to curves give the corresponding final phospholipid concentrations, which were 1, 2, 3, 4, 6, and 8 mmol SPC kg^{-1}. Inset: The corresponding absolute optical density. Lower panel: The mean hydrodynamic diameter of the mixed aggregates formed from the LUV (final concentration = 4.00 mmol SPC kg^{-1}) after addition of sodium cholate to the given total concentration (quasi-steady state, triangles, left axis). The diameter implied by an additional peak occurring at various positions between 300 nm and 900 nm, which is detectable in some samples with total cholate concentration above 9.00 mmol kg^{-1}, is not shown for better clarity. Circles give the intensity-normalised fraction of the peak corresponding to mixed lipid vesicles and/or other large mixed aggregates (right axis). In both panels, each data point represents a separate preparation. The standard deviation bars are only shown when they are larger than the corresponding symbol.

The dynamic light scattering yields qualitatively similar but quantitatively different results compared with the static light scattering (see Fig. 2). The dynamic light scattering curve pertaining to the LUV is generally shifted towards higher cholate concentrations relative to the static light scattering curve (cf. Fig. 2 lower *vs.* upper panel).

The dynamic light scattering uncovers coexistence of relatively small mixed micelles and much larger aggregates over a broad range of total cholate concentrations (Fig. 2, lower panel). The position of the peak pertaining to the large scatterers (including the mixed amphipat vesicles, the thread-like mixed aggregates, etc.) varies among the replicates of the same sample at high cholate concentration, however, as is reflected in the relatively large standard deviations illustrated in Fig. 2 (lower panel). We moreover detected an additional size-peak between 400 nm and 900 nm with the dynamic light scattering in an appreciable number of samples (data not included into Fig. 2 for better clarity). Taken together, this implies that large aggregates with different sizes and/or various shapes coexist during lipid (partial) solubilisation. They are not resolvable with the dynamic light scattering, as the available mathematical models for analysing the dynamic light scattering data presume similar geometry for all scatterers. We only calculated various

Table 1
The average diameter of the studied SPC vesicles[a], as determined with the dynamic light scattering.

	Mean diameter (nm)	Polydispersity index
LUV	121.8	≤0.13
IUV	82.8	≤0.16
SUV	44.1	≤0.24[b]

[a] Concluding from the published information pertaining to the used preparation method [38,39], less than 10% of the vesicles were oligolamellar.

[b] Increase of polydispersity index with diminishing average vesicle size reflects greater vesicle size-distribution skeweness upon approaching the minimum achievable vesicle diameter.

size values assuming spherical, rather than discoidal or thread-like, micellar shapes.) The average mixed micelle size generally decreases from ~14 nm to ~5 nm with raising total cholate concentration in the vesicle–micelle coexistence range.

3.1.2. Small unilamellar vesicles (SUV)

Small unilamellar vesicles (SUV) become slightly more optically dense after addition of small cholate amounts (optical density increases approx. 4–10% per 1 mmol total cholate kg^{-1}, see Fig. 3), in contrast to the situation found with the LUV. Further raising cholate concentration steeply increases the suspension optical density; the maximum value corresponds to nearly three times higher optical density for the cholate-containing *vs.* the original cholate-free preparation (Fig. 3). Increasing cholate concentration beyond such optical density maximum decreases the suspension optical density sharply to a quasi "plateau". This indicates essentially complete bilayer vesicle solubilisation into small mixed amphipat micelles. The solubilisation curve measured with the SUV shows no tailing in contrast to the LUV or the IUV curves (Figs. 2–4).

The average hydrodynamic diameter of the studied aggregates and the suspension optical density depend qualitatively similarly on total cholate concentration. Exceptional are only low cholate concentrations: addition of a small cholate amount changes little the hydrodynamic diameter of the mixed amphipat vesicles derived from the SUV (−2.0 nm); the measured optical density suggests a change in the opposite direction. Raising cholate concentration further then enlarges the mean diameter of mixed aggregates sharply, from 42 nm (essentially the starting value) to 102 nm, in qualitative agreement with the optical density data. Such changes more or less coincide with the first well-detectable small mixed micelle appearance.

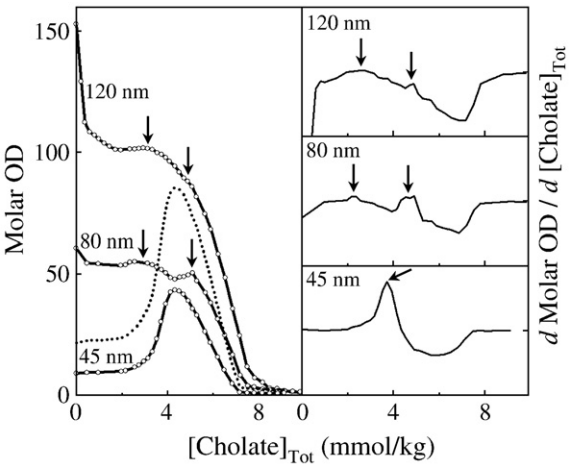

Fig. 4. Left panel: The molar optical density (quasi-steady state, $\lambda = 500$ nm) of the mixed aggregate suspension resulting from the LUV, the IUV or the SUV after addition of sodium cholate to the given total concentration (final SPC concentration = 4.00 mmol kg^{-1}). The curve pertaining to the SUV was calculated from the data measured at $\lambda = 400$ nm (dashed line) assuming $OD \propto \lambda^{-w}$ and $3.023 \leq w \leq 4.000$. Right panel: The derivative of the molar optical densities shown in the left panel vs. the total cholate concentration. The arrows point to unusual changes in optical density curves.

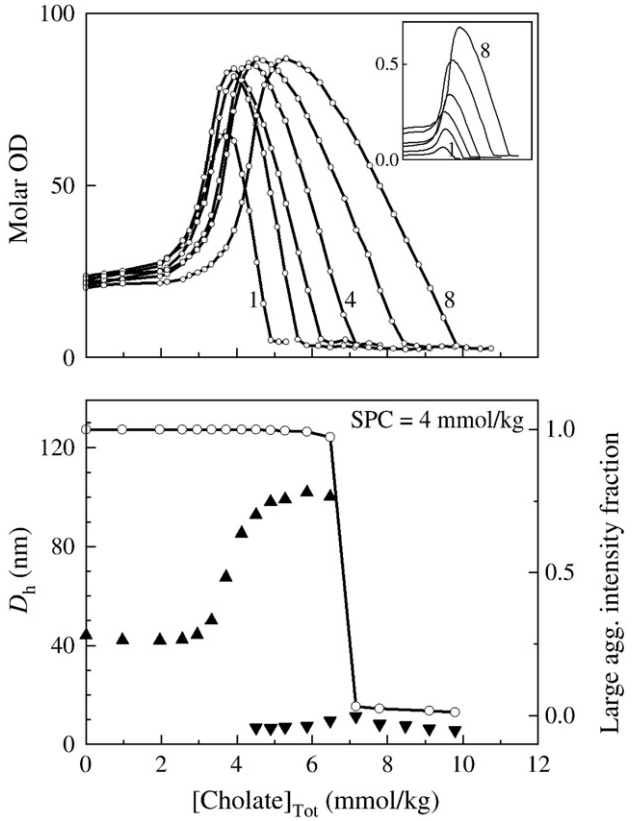

Fig. 3. Upper panel: The molar optical density (quasi-steady state, $\lambda = 400$ nm) of the mixed aggregate suspension resulting from the SUV after addition of sodium cholate to the given total concentration. The numbers next to curves give the corresponding final phospholipid concentrations, which were 1, 2, 3, 4, 6, and 8 mmol SPC kg^{-1}. Inset: The corresponding absolute optical density. Lower panel: The mean hydrodynamic diameter of the mixed aggregates formed from the SUV (final concentration = 4.00 mmol SPC kg^{-1}) after addition of sodium cholate to the given total concentration (quasi-steady state, triangles, left axis). A peak detectable in all samples with total cholate concentration above 6.50 mmol kg^{-1} somewhere in the range 90–350 nm is not shown for better clarity. Circles give the intensity-normalised fraction of the peak corresponding to mixed lipid vesicles and/or other large mixed aggregates (right axis). In both panels, each data point represents a separate preparation. The standard deviation is always smaller than the symbol.

The intensity-normalised fraction of the peak pertaining to the large aggregates falls steeply with increasing cholate concentration. The peak remains detectable at various positions between 90 nm and 350 nm, however (data not shown in Fig. 3 for better clarity). The average size of the small mixed phosphatidylcholine/cholate micelles is 5–11 nm. It suggests molecular control over the average small aggregate size. The dynamic and the static light scattering both imply similar solubilisation-endpoints.

3.1.3. Intermediate size vesicles (IUV)

Intermediate size vesicle (IUV) suspensions supplemented with a small amount of cholate become more transparent. We measured smaller optical density decrease with such intermediate-size (80 nm) unilamellar vesicles than with the LUV (note the slight increase observed with the SUV illustrated in Fig. 4). Raising cholate concentration further triggers a complex set of optical density changes. This is reflected in at least two well resolved, successive optical density *vs.* cholate concentration peaks. We detected two peaks—or more precisely: a peak with a shoulder—for the LUV as well. To determine these two peak positions for the LUV we had to take the derivative of optical density *vs.* total cholate concentration curves (see Figs. 2, 4). Escalating cholate concentration further decreases optical density of the suspension that originally contained IUV essentially in parallel with the optical density changes observed with the LUV and SUV suspensions. The process continues until the optical density reaches a low quasi-plateau, where most lipid vesicles are transformed into small mixed micelles. The gradual solubilisation creates a "tail" at the high end of optical density *vs.* cholate concentration curves. The tail is more prominent for the LUV than for the IUV and is not detectable for the SUV (Figs. 2–4).

It is therefore more appropriate to identify complete solubilisation with the cholate concentration at which the suspension optical density reaches its final, low value than by extrapolating the steeply descending part of the curves toward such a value. The minimum cholate

concentration needed to completely solubilise phosphatidylcholine into small mixed micelles evidently depends on the original vesicle size. It is generally higher for the larger than for the smaller vesicles (Figs. 2–4).

3.2. The time-resolved light scattering

Fig. 5 illustrates the temporal evolution of molar optical density of the LUV or of the SUV suspensions triggered by adding sodium cholate to the specified final concentration. The optically detectable vesicle-to-micelle transformation is sensitive to the initial average vesicle size, whether measured in quasi-equilibrium (the final quasi-steady state values provided in Figs. 2–4) or time-resolved.

Addition of a sub-solubilising cholate amount to the LUV suspension precipitously decreases the preparation optical density. The optical density reaches a final, constant value nearly instantaneously, indicative of fast partitioning of cholate molecules between the bulk and the LUV bilayers. Addition of a solubilising sodium cholate quantity to the LUV also promptly lowers the suspension optical density to approximately half the original value. The optical density subsequently decreases gradually toward the final very low value, which is reached after approx. 3–4 h (Fig. 5, left). The LUV solubilisation into small mixed-phosphatidylcholine–cholate micelles is thus a complex and relatively slow process.

The temporal optical density evolution in the cholate-supplemented SUV (Fig. 5, the right panel) differs from the corresponding time-course determined for the LUV suspensions. A sub-solubilising cholate addition triggers a small increase of the SUV optical density that seamlessly transitions into a smaller secondary decrease. Higher, but still sub-solubilising, cholate concentration (corresponding to the optical density maximum in Fig. 3) transiently lowers the suspension optical density. The suspension optical density thereafter continues to increase for at least 90 min. The final value is nearly three times higher than the original value, with a clear saturation tendency. Introduction of a solubilising sodium cholate amount, in contrast, precipitously decreases the suspension optical density. The subsequent asymptotic approach to the final value takes approximately 2 h. The secondary suspension optical density decrease possibly reflects diminution of the mixed amphipat micelles rather than vesicle solubilisation (cf. LUV, Fig. 5, left). We did not see the intermediate transition, characterised by the steep optical density increase, after having added the solubilising cholate amount to our preparations in a single step. The time-dependent and the continuously recorded optical density curves thus differ in this respect from the cholate concentration-dependent quasi-steady state changes illustrated in Fig. 3.

3.3. Quantitative analysis of the cholate-facilitated bilayer fluctuations

We analysed the data from Figs. 2 and 3 within the framework of the Helfrich bilayer elasticity model [40], which accounts for the functional dependency of the effective bilayer rigidity on the average vesicle size. This afforded the effective bilayer rigidity as a function of total cholate concentration, based on the observed LUV diameter diminution (see Appendix B and Table 2, which expresses the results as a function of total cholate concentration). We then inferred the apparent size and optical density of the SUV preparations from the LUV results without making any further assumption. The qualitative agreement between the calculated and the measured results for the SUV shown in Fig. 6 gives some credence to the underlying assumptions. To improve the agreement further one could allow for the relatively large polydispersity of the SUV as compared with the LUV into the model.

4. Discussion

4.1. Experimental considerations

Under the physiologic conditions cholate is essentially an anionic biosurfactant with the aqueous dissociation constant $pK_a = 4.63$ (25 °C, 150 mM ionic strength [44]). The apparent dissociation constant of cholate is higher, however, in the homo-aggregates that prevail above this biosurfactant CMC and in the presence of other lipids or surfactants, which tend to form hetero-aggregates with this biosurfactant. The chief reasons are the lower polarity and the repulsive electrostatic potential at such aggregate surface (see Appendix A). Our own potentiometric measurements ([45] and other unpublished data) suggest that $pK_a = 4.80$ (37 °C, 150 mM ionic strength) for an aqueous cholate solution below CMC and that cholate bound to the originally electroneutral SPC bilayers has a higher logarithmic dissociation constant: $pK_a^{mem} = 6.91$ (37 °C, 150 mM ionic strength). Our results are similar to the values that had been reported earlier based on the ^{13}C NMR of the membrane-bound cholate [46,47].

We wished to experiment only with cholate in a well defined ionisation state. We therefore adjusted the studied suspensions pH so as to ensure complete ionisation of the dissolved as well as the aggregate-bound cholate. We met the goal—and ensured >99% cholate ionisation for all the tested lipid and surfactant concentrations—by experimenting at $pH = 10.25 \gg pK_a^{mem} + 2$ (see Appendix A for further discussion). Previous studies of the membrane-associated cholate were conversely

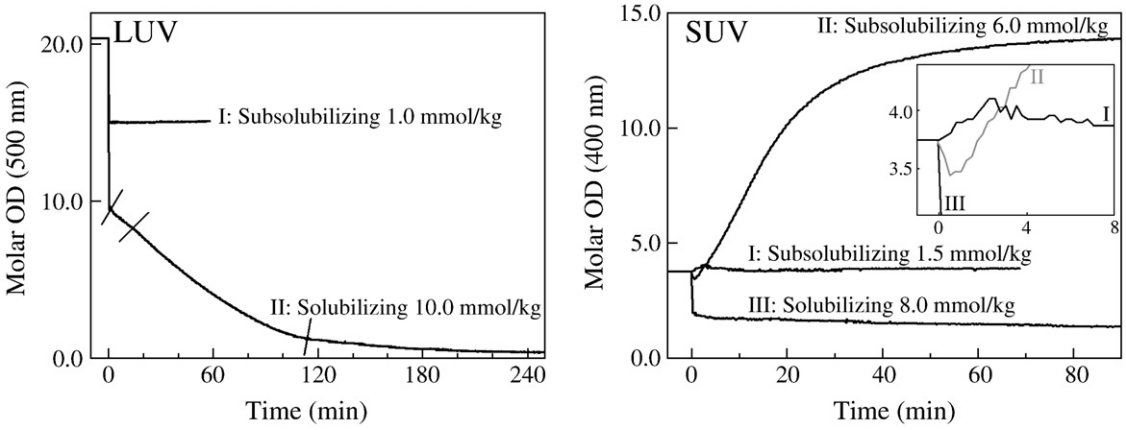

Fig. 5. The temporal evolution of molar optical density of the LUV (left panel) or the SUV (right panel) suspensions after addition of sodium cholate to the given total concentration (final SPC concentration = 4 mmol kg^{-1}). The baselines are corrected for the dilution effect. The curve II in the left panel is subdivided into four segments by the crossing lines indicating the apparent changes in optical density decrease rate. Inset: Magnification of the changes taking place during the first few minutes.

Table 2
The calculated bending rigidity, κ, of the mixed amphipat bilayers as a function of total cholate concentration. The results are derived from the LUV size changes measured with the static and dynamic light scattering and analysed with the basic Helfrich's model (Appendix B) [40].

$[Cholate]_{Tot}$	Static light scattering		Dynamic light scattering	
	Molar OD	$\kappa\ 10^{-20}$ J (k_BT)	D_h nm	$\kappa\ 10^{-20}$ J (k_BT)
0.000	153.004	–[a]	121.8	–[a]
0.383	112.509	1.031 (2.5)	107.1	0.807 (2.0)
0.973	105.622	0.846 (2.1)	106.0	0.732 (1.8)
1.464	102.489	0.783 (1.9)	104.5	0.664 (1.6)
1.947	101.072	0.766 (1.9)	98.5	0.518 (1.3)

[a] We know of no published bending rigidity value for the pure SPC bilayers. The reasonably similar egg PC has $\kappa \approx 9.7$–$13.4\ k_BT$ [41,42]. Reliable values for the fluid-phase PCs typically range between 10 k_BT and 20 k_BT, depending on chain-length and -unsaturation [43]. Dilinoleyl-phosphatidylcholine with four double bonds per molecule has $\kappa \approx 11\ k_BT$ [43]. We therefore presume $\kappa \approx 15\ k_BT$ (6.172×10^{-20} J) for the studied simple SPC bilayers.

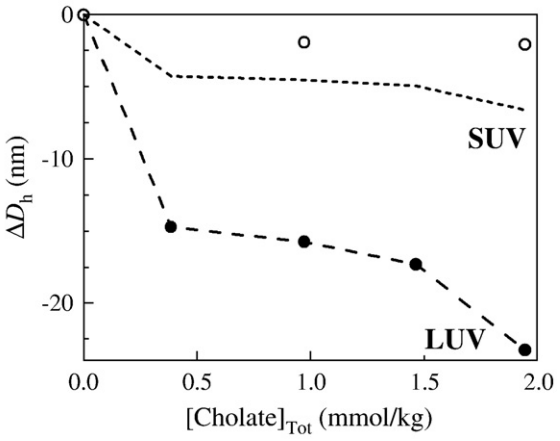

Fig. 6. The cholate (total concentration = 0 − 2 mmol kg^{-1}) induced (mixed) vesicle hydrodynamic diameter changes (4.00 mmol SPC kg^{-1}). Symbols give the experimental data and lines the values calculated as is described in Appendix B with the bending rigidity values given in Table 2. The calculation presumed the same cholate apparent partition coefficient in the LUV and the SUV bilayers at similar cholate concentration.

done nearly exclusively in the quasi-physiological range $6.5 < pH < 7.5$ (i.e. around pK_a^{mem}). This focused on the physiologic cholic acid/cholate-lipid interactions but aggravated proper analysis of cholate partitioning/binding. Indeed, no previous study of which we know has treated the pH effects in such range properly (i.e. by correctly considering both the dissolved as well as the lipid-associated cholate ionisation). Most importantly, the variability of cholate ionisation in such pH range was in the previous publications accounted for only incompletely, if at all.

The experimental pH effects on cholate ionisation are greatest when $pH \approx pK_a^{mem}$, i.e. around the physiological pH range.[1] This explains some discrepancies between the various published results. For a similar reason, the Coulomb correction in such pH range is requiring utmost care: incomplete cholate ionisation, a consequence of the small pH–pK_a^{mem} difference, would make mathematical analysis of the resulting data much more complex [45]. One should also carefully consider the local pH shift, ΔpH, which results from proton attraction to the negatively charged surface. Indeed, cholate is fully charged only when the interfacial pH sufficiently exceeds the interfacial pK_a^{mem}. One must therefore choose the bulk $pH \geq pK_a^{mem} - \Delta pH + 2$ (or 3) rather than the bulk $pH \geq pK_a + 2$ (or 3) to ensure full ionisation of the biosurfactant and thus a reasonably simple mathematical analysis of experimental data (see Appendix A for further discussion).

Wanting to ensure cholate equilibration in the tested suspensions, we sought to achieve constancy of the measured signal by waiting long enough. We kept in mind that the minimum required time depends on the initial vesicle size as well as on total cholate and lipid concentrations (Fig. 5). Cholate exchange and equilibration between an aqueous solution and a lipid bilayer can be slow at pH = 10.25. The time needed by cholate to cross a lipid bilayer and then to equilibrate between the outer and the inner membrane half is, at least in a pore-free bilayer, quite long. Addition of cholate may moreover initially (and often transiently) decrease the dispersion optical density, which subsequently re-increases, or vice versa (Fig. 5). Premature read-out is thus prone to produce wrong conclusions. We consequently either equilibrated each test sample until its optical density was constant, which took up to 6 h, or else measured the full time-dependency.

We also cared about SPC hydrolysis at the high chosen experimental pH. We first calculated the rate of phosphatidylcholine degradation based on published information [48,49] and duly considering the local pH-shift effects (see Appendix A). We concluded that the overall degree of lipid hydrolysis should be less than 2.5% during the 6 h equilibration period at pH = 10.25, $T = 25$ °C, $I = 150$ mM, except when the mole fraction of bound cholate in the aggregates is less than 0.1. This would apply for our suspensions (SPC concentrations ≤ 6.00 mmol kg^{-1}) only if the total cholate concentration is less than 1.4 mmol kg^{-1} (see the published partition coefficient values of refs. [50,51]). Such mixtures require equilibration times of a few minutes (Fig. 5), however. This is too short to cause considerable degradation. We furthermore checked experimentally that phospholipid hydrolysis did not play a role in our experiments. To this effect we confirmed that the lysophosphatidylcholine level in several representative samples, kept at pH = 10.25 and T = 25 °C for 6 h, was below the HPLC method detection limit. No phosphatidylcholine concentration change could be also detected. We therefore deem our results to be reliable and not falsified by phospholipid degradation.

4.2. Supramolecular view of the cholate-induced vesicle-to-micelle transformation

In contrast to micelle-to-vesicle transition, which is well characterised structurally and kinetically [52–55], the reverse process of vesicle-to-micelle transformation is not yet fully understood [1–3,5,18,19,21,22,24,29,56]. The associated data interpretation is correspondingly diverse and mainly phenomenological.

The most common description of vesicle-to-micelle transformations is the "three-stage model" [3]. According to such model, at stage I surfactant monomers partition into lipid bilayers. Higher surfactant concentration pushes the mixed amphipat suspension into stage II at which the lipid-saturated micelles coexist with the surfactant saturated vesicles, according to the model. At stage III only micelles exist.

Despite its simplicity, the three-stage model can describe reasonably well the basic behaviour of many lipid–surfactant mixtures. This explains the model popularity despite its restriction to just two, in detail unspecified, aggregate types: bilayer vesicles and micelles. The three-stage model cannot cope with the structural diversity of the data described by many researchers [24,56–58] including ourselves. Indeed, such data suggest that surfactants solubilised bilayer vesicles in a continuous process comprising at least two sequential and partially overlapping, structurally complex, and aggregate size-dependent phenomena—one increasing and the other decreasing average mixed aggregate size (see Appendix D).

Fig. 7, which we construed on the basis of our own and previously published findings, illustrates the most typical structures that may (co)exist during vesicle transformation into ultimately small mixed micelles. The figure also highlights the only unambiguous and common boundary in such a transition: the complete replacement of the relatively large, water-filled bilayer vesicles (whether spherical and non-perforated or not) by the much smaller and more compact

[1] For illustration: degree of ionisation varies between 24–76% at $pH = pK_a \pm 0.5$.

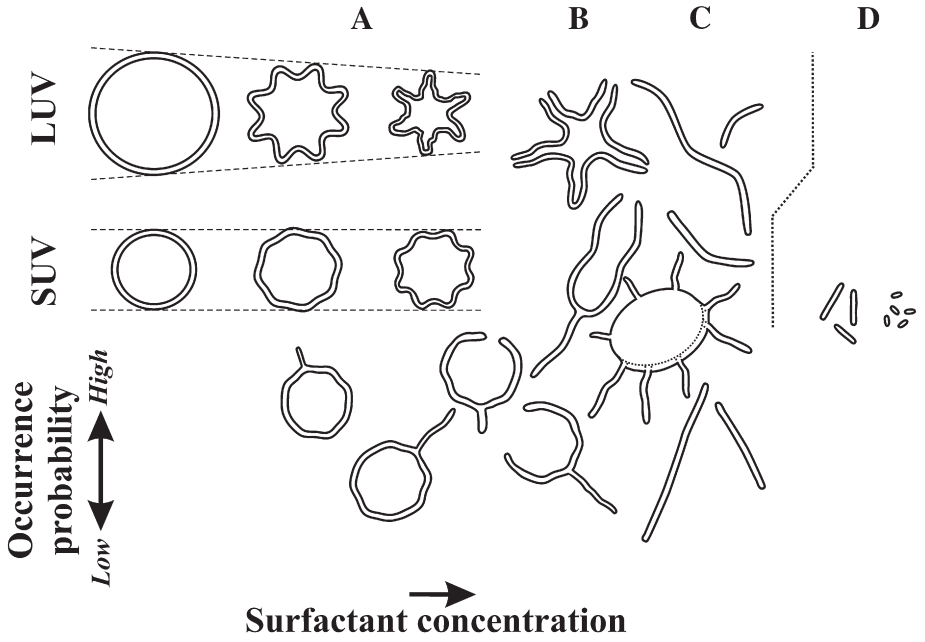

Fig. 7. Schematic representation of the most typical structures that can appear, and typically coexist, during progressive vesicle-to-micelle transformation, and their ad hoc separation into four quasi-distinct regions: the bilayer vesicle/mixed vesicle region (A); the open, quasi-lamellar structure region (B); the long, thread-like micelle region (C); and the relatively small micelle region (D).

micelles (whether thread-like, ellipsoid, discoid, or spherical). Any further firm subdivision is artificial and *ad hoc*, even if it facilitates the underlying process description. In the following we thus reduce the general, quasi "bicontinuous and parallel transformation", which we advocate herein, to just four transformation steps or regions: A, B, C, D (Fig. 7). We caution the reader that this serves solely better comparability with the three-stage model and that such simplified "differentiation" has no one-to-one correlation with reality. For further commentary see Appendix D.

4.2.1. The lamellar bilayer vesicles/mixed amphipat vesicles (region A)

Low total cholate concentrations result in a low degree of cholate–bilayer association. Only mixed amphipat bilayer vesicles then exists. If cholate–bilayer association was the only process involved, the average vesicle size would therefore simply increase with cholate concentration [59], owing to the growing number of molecules in each vesicle. Evans et al. [59] showed that the surface area of a pressurised giant unilamellar vesicle increases monotonously with the added/bilayer bound bile acid fraction. In reality, we measured a "richer" and vesicle size-dependent optical density *vs.* total (low) cholate concentration curve: the slope of our experimental curve is first steep and negative for the LUV, less negative for the IUV, and slightly positive for the SUV. At slightly higher cholate concentrations the slope is positive for all the investigated vesicles (cf. Fig. 4, left panel).

Our dynamic and static light scattering data qualitatively agree for the SPC/cholate mixed aggregates originating from the LUV. This confirms that the apparent mean diameter of such aggregates decreases with increasing total cholate concentration (Fig. 2). Conversely, the dynamic light scattering indicates a slight vesicle size decrease (~2.0 nm) for the SUV whereas the static light scattering in parallel reveals a slight increase of the SUV size (Fig. 3). The diversity of bilayer forms, which are brought about by phospholipid–cholate interaction and association, evidently increases with the average aggregate size even if the starting vesicles are always spherical.

Surfactant insertion into a lipid bilayer lowers the resulting mixed bilayer rigidity [60,61]. This lowers mechanical bilayer stability [59] and facilitates bilayer fluctuations [62,63]. Hydration studies with mixed bilayers [62] and high-intensity dark-field micrographs [63] vindicate the claim. The frequency spectrum of bilayer fluctuations inevitably depends on the average vesicle surface/size, and is more restricted for the SUV than for the LUV. The size-dependent counterplay between the bilayer expansion caused by cholate adsorption and the apparent bilayer vesicle shrinkage caused by the cholate-induced bilayer fluctuations can thus explain our quantitative conclusions summarised in Fig. 6. Absence of such fluctuations in mixed amphipat vesicle under tension in turn explains the monotonous size-increase with surfactant concentration reported by Evans et al. [59].

Surfactant insertion into lipid vesicles lowers bilayer bending rigidity [11,59,60,64,65]. With an improved vesicle adaptability assay, Wachter et al. [66] have assessed the bending rigidity of the SPC bilayers saturated with the non-ionic surfactant polyoxyethylene (20) oleyl ether ($C_{18:1}EO_{20}$) and concluded that it is $\kappa \approx 2.1\ k_BT$. Brown and colleagues [64] estimated from the deuterium NMR relaxation times the bending rigidity of the 2/1 dimyristoyl-phosphatidylcholine/$C_{12}EO_8$ mixed bilayers, which is also not too far from phospholipid solubilisation, to be $\kappa \approx 7\ k_BT$. Evans, et al. [59] reported a quasi-exponential decrease of bilayer lysis tension with increasing concentration of the trihydroxy bile acid cholylglycine in egg phosphatidylcholine giant vesicle. Their data imply bilayer bending rigidity at 5–10% of the saturation limit also to be in the 5–8 k_BT range. Our own estimate of $\kappa \approx 2\ k_BT$ (Table 2) for the suspensions containing sub-solubilising cholate concentrations is therefore probably too low, unless some impurity in the employed SPC acted in synergy with cholate to lower the mixed bilayer bending rigidity. We find this unlikely.

The low calculated κ value therefore points towards an alternative and preferable explanation: an inhomogeneous surfactant distribution within the fluctuating mixed amphipat bilayers [11,65]. Such distribution introduces another surfactant-sensitive size dependency into the generalised Helfrich's model, in addition to the size-dependent fluctuation cut-off. A finite surface area namely restricts the range of all possible vesicle membrane fluctuations. In turn, this diminishes the maximum surfactant-induced κ-decrease and the resulting apparent vesicle size reduction. Laterally and transversely non-uniform surfactant distribution can account for the 25% discrepancy between the cholate-induced size changes of the LUV and SUV, which we measured with the dynamic light scattering (Fig. 6) (to explain the much larger difference between the static light scattering changes measured with the LUV or SUV one would have to allow for

the putative cholate-induced bilayer refractive index change (e.g. due to bilayer hydration) and/or for bilayer thickness variation).

Restricted transbilayer "flip–flop" of charged cholate molecules through SUV bilayers could play a role as well. Cabral et al. [67] assessed the rate of cholate flip–flop through egg phosphatidylcholine SUV bilayers (diameter ~23 nm) with the ^{13}C NMR; the charged cholate molecules at pH = 10 practically failed to traverse such bilayers (flip–flop half-time > 24 h at 35 °C). Donovan and Jackson [68] investigated surfactant flip–flop through LUV bilayers by monitoring the time-dependency of surfactant binding. They determined the transverse time of the ionised bile salts across lipid bilayers to be hours or even minutes [68]. The discrepancy could reflect vesicle size differences; the relatively high SUV bilayer curvature creates a less favourable surrounding (higher chemical potential) on its inside for charged surfactant molecules as compared with the outer bilayer half. Cholate resistance towards "running uphill" through the SUV bilayer could therefore explain the slower flip–flop through the highly curved SUV bilayers as compared with the "flatter" LUV bilayers. The same applies to some of the differences illustrated in Figs. 2–4, at least.

4.2.2. Vesicle poration, partial fragmentation, and/or fusion/appearance of thread-like micelles (region B)

The differently large vesicles respond differently to cholate incorporation in the intermediate cholate concentration range (for illustration: total cholate concentration of 2.0–4.5 mmol kg^{-1} for the samples with SPC concentration of 4.00 mmol kg^{-1}, Figs. 2–4). Optical density of the originally LUV and the originally IUV suspensions responds to surfactant concentration within such range only a little. For a better visibility and experimental resolution we therefore differentiated each curve (see the right set of panels in Fig. 4). This confirmed existence of two optical density maxima for the LUV (for the LUV, better described as a peak and a shoulder) as well as for the IUV. Optical density of the suspensions that originally contained the SUV, in contrast, comprised only one optical density peak (within resolution of our measurements), with a maximum at nearly three times the initial optical density value.

The first maximum in our optical density *vs.* cholate concentration curves is visible at approximately the same total surfactant concentration for the originally LUV and IUV suspensions (Fig. 4). This suggests that the surfactant-dependent bilayer expansion in sufficiently large bilayer aggregates dominates over the surfactant-induced bilayer fluctuations. In contrast, our data can neither support nor exclude the previously proposed shedding of SUV during solubilisation of the originally LUV/IUV SUV, which had been implied for phosphatidylcholine–octylglucoside mixtures [58,69].

The shoulder on the molar optical density *vs.* total cholate concentration curve measured with the LUV, the second peak on such curve for the IUV, and the single peak on the curve for the SUV all correspond. They moreover coincide with the first detection of the small mixed micelles by the dynamic light scattering. Such "secondary characteristics" of optically measured solubilisation curves thus reveal onset of vesicle solubilisation; they depend on initial vesicle size, showing a higher maximum for the smaller than the larger vesicles.

The dynamic light scattering data basically confirm the static light scattering results. The peak corresponding to the large aggregates shifts upward with increasing cholate concentration (Figs. 2–3). The dynamic light scattering detects small mixed micelles at lower cholate concentrations for the SUV than for the IUV or the LUV. The dynamic light scattering delivers only imprecise information about the large aggregate size within the bilayer presolubilisation region (i.e. at the higher end of intermediate cholate concentrations range; Fig. 2); this suggests coexistence of various aggregate forms (Fig. 7). An additional peak between 90 nm and 900 nm in some measurements (data not shown) supports the conclusion. These findings justify the bilayer solubilisation illustration presented in Fig. 7.

Walter et al. [24] investigated the intermediate structures in vesicle–micelle transition of a phosphatidylcholine SUV–cholate system with cryo-transmission electron microscopy. For the cholate concentrations which increase the suspension optical density most steeply (the ascending part of optical density "peak") they observed open vesicles, collapsed vesicles, bilayer patches, and cylindrical (i.e. thread-like) micelles. They also detected some cylindrical mixed micelles at the broken vesicle/large bilayer sheet rims. Walter and colleagues reported maximum prevalence of such micelles for the cholate concentrations corresponding to the optical density peak illustrated in our Figs. 2–4. Vinson et al. [34] saw similar structures with the LUV phosphatidylcholine–octylglucoside mixtures.

Long et al. [20] investigated the reverse process, i.e. the intermediate aggregate formation by diluting lecithin–bile salt micellar suspensions. Their small-angle neutron diffraction data revealed coexistence of bilayer vesicles and cylindrical micelles even in some samples for which dynamic light scattering measurements showed just one kind of aggregates. They explained the discrepancy observed at intermediate cholate concentrations by postulating that micelles are too long to be distinguishable from bilayer vesicles with the visible light. Existence of such micelles or (micellar) protrusions emerging from bilayers during vesicle solubilisation also can explain the variable peak position which we uncovered for the large aggregates with the dynamic light scattering.

We combined these findings with the published information on vesicle leakage [2,18,22] and our own conclusion and kinetic observations to construct the generalised scheme of vesicle-to-micelle transformation which we present in Fig. 7.

In our view, the changes occurring in this region, reflected by the static and dynamic light scattering measurements (Figs. 2–4), result from the gradual bilayer enrichment and finally saturation with the surfactant and the accompanying diversity of transformations in the mixed aggregate morphology. The two major types of such morphological changes are: vesicle poration/rupture into quasi-lamellar open vesicle/bilayer fragments, on the one hand, and retro-fusion of the resulting fragments or vesicles into larger aggregates, on the other hand. The most frequent minor and/or transient change is protrusion formation, which is optically indistinguishable from vesicle fragment fusion. It stands to reason that the protrusion formed before creation of transbilayer pores (which permit fast cholate migration across bilayers) involve just the outer bilayer half; subsequently (after the porated or fragmented bilayers stop acting as barriers to cholate transport) both bilayer halves are involved. Complexity of the derivatives shown in Fig. 4 supports our overall picture of vesicle-to-micelle transformation (Fig. 7). It moreover proves that the process of surfactant-induced vesicle solubilisation is not interchangeable with the vesicle formation triggered by decreasing surfactant concentration. Whereas the latter is exclusively controlled by the mixed aggregate composition [70–73] and its change-rate [74,75], the former depends on the starting aggregate size, on total amphipat concentration, and also on equilibration time (Figs. 2–5).

Arguably, each aggregate shape transformation triggers a time- and morphology-dependent local cholate concentration adjustment, whether this is directly observable or not. Such an adjustment can give an explanation for the initial light scattering variation and/or its transience in the case of the SUV (see Fig. 5) as well as the preferential occurrence of the long cylindrical mixed micelles at bilayer fragments' rim (see the previous paragraphs and [24]). Unfortunately, the optical light scattering was only capable of directly and unambiguously confirming the local cholate concentration increase in the caps of the thread-like, mixed phosphatidylcholine–cholate micelles (Fig. 8). The size- and time-dependency of the scattered light characteristics measured with the partially solubilised phospholipid (Figs. 2–5) implies a similar cholate local concentration adjustment in the pre-solubilisation region, however.

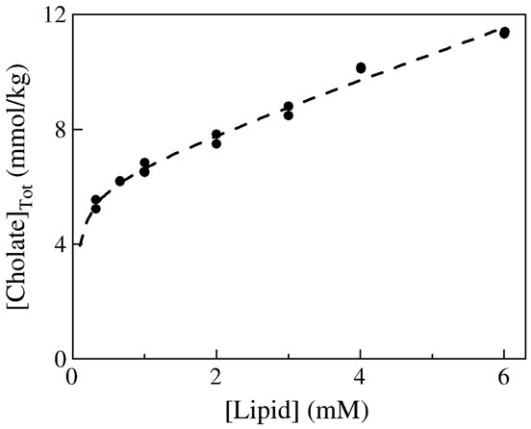

Fig. 8. Total cholate concentration required to solubilise the LUV bilayer vesicles into small mixed amphipat micelles as a function of total phospholipid (SPC) concentration. Symbols represent the experimental static light scattering data. The dashed curve illustrates the best fit, derived from the model proposed by Roth et al. [76] with the modifications described in Appendix C.

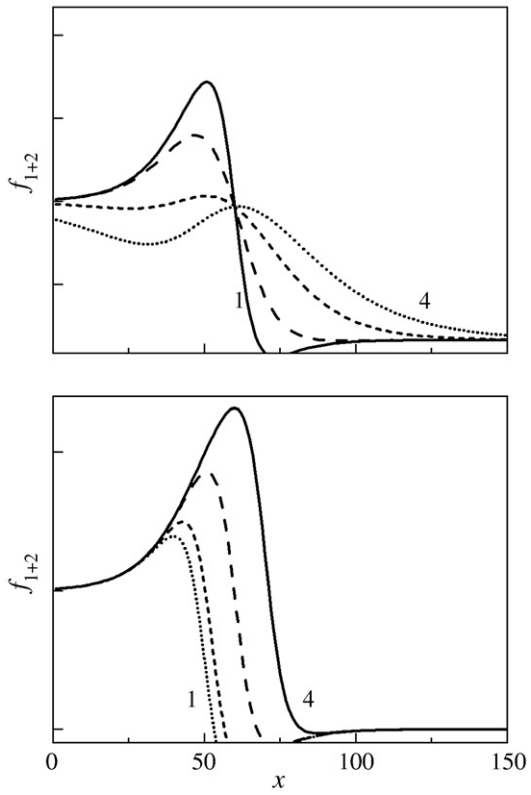

Fig. 9. The sum of two sigmoidal curves, described by Eqs. (D1)–(D2), can mimic all the basic forms of the experimental optical density *vs.* cholate concentration curves which we measured. More specifically, we always used $n=1.5$ together with $x_0=50$, $S=0.1$, $dx_0=10$, and $dS=-0.05$, -0.025, 0.05, and 0.2 (for the curves 1 to 4, respectively) to generate the set of curves shown in the upper panel or $x_0=50$, $S=0.1$, $dx_0=0$, 2.5, 10, and 20 (for the curves 1 to 4, respectively), and $dS=0.2$, to create the set of curves in the lower panel.

Our data indicate that the propensity for large aggregate or protrusion formation depends on several parameters. The starting aggregate size can obscure their identification and experimental data interpretation, however: the aggregates originating from the LUV scatter light similarly as the LUV containing less cholate (i.e. region A, Fig. 7) while optical density of the suspension of the mixed amphipat aggregates stemming from the SUV exceeds the optical density of the original SUV suspension. The optical density peak measured with various vesicle preparations consequently increases with decreasing initial vesicle size (Fig. 4). Both the shape and the height of the molar optical density peak depend on lipid concentration (Fig. 3) as well, which can affect the transformation kinetics too. Aggregate proximity/higher amphipat concentration raises the probability for both aggregate–cholate as well as aggregate–aggregate collisions and fusion. This facilitates protrusion growth and aggregates re-merging/reformation/fusion, any of which increases the suspension optical density. This offers an explanation for the flatter optical density vs. cholate concentration curve measured at the relatively high lipid concentrations. The starting aggregate size effect on the average inter-aggregate distance moreover explains why such effect is greater for the LUV than for the SUV (Figs. 2, 3). Lack of accurate cholate–aggregate association constant values prevented us from analysing this dependency quantitatively.

We warn against accepting any of the reported "vesicle saturation" with a surfactant boundary, the derived effective bound molar fraction, x_e^{sat}, or the associated effective bound molar ratio, R_e^{sat}, as a reliable and/or definitive value, at least when such parameters are derived from the optical light scattering data. The long cylindrical, thread-like micelles may coexist with the mixed vesicles at surfactant concentrations below the optical density "peak". Some open vesicles may coexist with the cylindrical micelles at the beginning of the ascending part of the optical density peak. The starting size-dependency of suspension optical density changes may moreover shift the optical density peak position between various preparations with identical composition and different morphology (see Figs. 4, 9 and Appendix D). All these phenomena are evidently due to bilayer curvature effects and arguably a consequence of an uneven surfactant distribution between and within the mixed amphipat aggregates with different average and local curvatures.

4.2.3. Thread-like micelle fragmentation/small cylindrical and/or spherical micelle formation (region C)

Increasing cholate concentration well above the concentration that ensures full bilayer fragmentation shortens the thread-like micelles. The cylindrical micelles thus ultimately transform into the smaller ellipsoidal or (quasi) spherical micelles. In parallel, the suspension optical density decreases, diagnostic of (nearly) complete lipid solubilisation. The weight fraction of the peak corresponding to the small micelles in the dynamic light scattering data concurrently increases and the weight fraction of the peak corresponding to the large/long aggregates decreases (Figs. 2–3, right axes). The suspension characteristics which we have determined for the region C are thus qualitatively the same as those measured previously with the visible light scattering and neutron diffraction moving in the opposite direction, i.e. starting with the small mixed amphipat micelles and then triggering larger aggregate formation by lowering total surfactant concentration [70].

The tailing of optical density *vs.* cholate concentration curve depends on the initial vesicle size. It is more prominent for the mixtures originating from the LUV (data published by de la Maza and Parra[18], who worked with larger vesicles than our LUV show also tailing) than for the preparations originating from the IUV (Figs. 2, 4). Our data pertaining to the SUV show no clear tailing (Figs. 3–4), however.

Temporal evolution of the optical density measured after addition of a solubilising cholate amount elucidates the observation. LUV solubilisation, as reflected in the temporal optical density evolution, follows a similar pattern as the cholate-induced concentration-dependent changes (Figs. 2, 5); one can thus view the LUV solubilisation as a gradual but rather rapid aggregate transformation. In contrast, the SUV seem to be less capable of accommodating large amounts of cholate, probably owing to their smaller average surface area that only tolerates a limited fluctuation spectrum; the flip–flop hampering surface curvature influence may play a role as well. Small vesicles therefore break more directly into cylindrical micelles, and require a lower total cholate concentration for solubilisation, than the LUV (Figs. 2–4).

Turbidimetric/optical density measurements can quantitatively and reliably reveal the effective surfactant mole fraction above which only small ellipsoidal or spherical micelles exist, x_e^{sol}. We evaluated such fraction from the data given in Figs. 2–4 with the mathematical approach of Roth et al. [76]. We thus accounted for the micelles' finite size and the inhomogeneous end-caps (inhomogeneous with regard to surfactant and lipid distributions at both ends as compared to the central part of each cylindrical micelle). We moreover included the Columbic interactions into the model (Appendix C) and present the results in Table 3 and Fig. 8. The predicted non-linearity at low lipid concentrations agrees with the experimental data measured with the LUV (<1.00 mmol SPC kg^{-1}). We were unable to collect similar data with the dilute SUV preparations owing to their low scattering intensity. From the whole experimental data set we were nonetheless able to conclude that the effective surfactant molar ratio in the aggregates at complete lipid solubilisation is lower for the SUV than for the LUV: $R_{e,SUV}^{sol} < R_{e,LUV}^{sol}$. The size of the small mixed micelles existing at such boundary is moreover larger for the SUV ($2r = 11.4$ nm) than for the LUV ($2r = 4.5$ nm). This supports our earlier conclusion that the SUV, having a relatively small surface area and restricted flip–flop ability, can tolerate less cholate than the LUV. The SUV therefore requires less cholate to break into larger and having lower R_e mixed micelles (see Figs, 2–4, Table 3).

4.2.4. The small mixed micelles (region D)

A high cholate concentration in a lipid suspension ensures that all the aggregated amphipat molecules will form only small mixed amphipat micelles (Fig. 2, 3). Adding a solubilising cholate amount to either the LUV or the SUV triggers a slow terminal optical density decrease, diagnostic of the progressive micelle size diminution (Fig. 5).

5. Conclusions

We characterised various soybean phosphatidylcholine–sodium cholate mixtures with light scattering techniques to elucidate vesicle-to-micelle transformation. More specifically, we used the static, the time-resolved, and the dynamic light scattering to investigate the equilibrium optical density and aggregate size in soybean phosphatidylcholine suspensions supplemented with cholate. We worked with unilamellar vesicles blended with fully ionised sodium cholate at pH = 10.25. We varied lipid concentration, starting with the lowest properly explorable value of 1 mmol kg^{-1}, and also changed cholate concentration, as have been done by many researchers before. Additionally and importantly, we explored the starting vesicle size ($2r_v = 45$ nm–120 nm) effect to explore the influence of lipid bilayer curvature on lipid solubilisation and mixed micelle formation.

The size-standardised measurements uncovered several new features. For example, we have now found out that the cholate-induced initial vesicle size decrease is greater for the originally large than for the originally small vesicles. Quantitative data analysis confirmed that the difference is mainly due to the broadening of shape-fluctuation spectrum with the mixed bilayer vesicle surface area. In contrast, we found the suspension optical density increase before complete vesicle solubilisation to be bigger for the originally small than for the originally large vesicles. The small, 45 nm vesicles thus require around 30% less cholate for complete solubilisation than the larger, 120 nm vesicles. Surprisingly, the former nonetheless form approximately twice as large mixed amphipat micelles.

Simple phenomenological parameterisation of optical density *vs.* total cholate concentration curves suggests that vesicle-to-micelle transformation size-wise predominantly involves two largely parallel phenomena. It stands to reason that the first is associated with an apparent, gradual aggregate size decrease; it involves progressive bilayer destabilisation, bilayer fragment- and detached thread micelle formation, and finally micellar diminution. The second process increases the apparent aggregate size; it mainly involves bilayer fusion or vesicle reformation and/or formation of bilayer-attached thread-like protrusions.

From the morphological viewpoint, the originally spherical vesicles arguably become aspherical due to surfactant incorporation. The reason is cholate-dependent bilayer softening and enhancement of bilayer fluctuations, which promotes irregular vesicle forms. The mixed amphipat vesicles compensate for some of the excess area that results from the surfactant binding to the outer bilayer half by forming thread-like protrusions. Arguably, the surfactant concentration at the end of any relatively thin structure is higher than in the less curved cylinder or bilayer part. It furthermore stands to reason that aggregate surface fluctuations provoke inhomogeneous surfactant distribution in the mixed amphipat bilayers. The resulting local surfactant accumulation catalyses transbilayer pore formation, more frequently and/or likely when lipid-solubilising surfactant concentration is approached. Strong fluctuations/protrusions and/or pores increase the probability for, first, vesicle re/fusion and, second, bilayer fragmentation.

Our experimental observations are at least semi-quantitatively in accord with the prevailing theoretical bilayer elasticity model results. The available models would have to be refined (or combined with further theories) to describe our findings completely and quantitatively. This remains to be done.

The popular three-stage bilayer solubilisation model is convenient but potentially misleading. For better accuracy and broader applicability we advocate replacing it with the more realistic continuous (i.e. bicontinuous and parallel) transformation model, in which aggregate curvature plays an important role. The starting vesicle size effect precludes determination of bilayer-saturating surfactant concentration from light scattering or size results alone. More fundamentally, any such concentration value is an ill-defined quantity, due to inhomogeneous surfactant distribution along (and across) the mixed aggregate surface.

The presumption of constant and laterally uniform aggregate composition is not tenable in any solubilisation model, owing to interdependency of local aggregate composition and curvature. This causes small vesicles to solubilise more readily than large bilayer aggregates, and then surprisingly to form (at least for some time) relatively large mixed micelles. Inhomogeneous surfactant distribution moreover helps explain—together with the bilayer barrier to surfactant transport—why a vesicle-to-micelle transition is not simply a mirror

Table 3
The mixed aggregate composition, the corresponding aqueous cholate concentration, and the cholate partition coefficient into the mixed aggregates at the total cholate concentration ensuring complete soybean phosphatidylcholine solubilisation into small mixed micelles[a]. The values are derived from the static light scattering data using the analytical approach described by Roth et al. [76], with allowance for the Coulomb interactions (see Appendix C).

	R_e^{sol}	$[Cholate]_w$[a] (mM)	$[Cholate]_{w,int}$[a] (mM)	A_w[a] ($mM^{3/2}$)	R^2	P_0[a]
LUV	0.877 ± 0.058	6.65 ± 0.35	0.23 ± 0.01	0.88 ± 0.26[d]	0.988	1.1×10^5
SUV[b]	0.709 ± 0.042	4.31 ± 0.35	0.16 ± 0.01	0.10 ± 0.35	0.996	1.4×10^5
SUV[c]	0.624 ± 0.020	5.08 ± 0.07	0.23 ± 0.00	0.88	0.994	9.5×10^4

[a] $[Cholate]_w$ is the bulk aqueous cholate concentration. $[Cholate]_{w,int}$ is the aqueous cholate concentration at the aggregate surface, corrected for the Coulomb effect. A_w is a fitting parameter that takes into account the micellar scission energy. P_0 is the partition coefficient of cholate into the phosphatidylcholine–cholate mixed aggregates.

[b] Owing to the low scattering intensity of the aggregates formed from the SUV, we were unable to conduct measurements with highly diluted SUV. This precluded us from studying the deviation from linearity at low lipid concentrations and thus from accurately calculating the $A_w$value for the SUV; the mentioned value is likely underestimated.

[c] Calculations done with the A_w derived from the LUV data, for at least a rough approximation.

[d] The result corresponds to a scission energy of $2\epsilon = 9.5$–$10.0\ k_BT$, if $0.2 < R_e^{sat} < 0.35$. Roth et al. [76] obtained a higher value for octylglucoside ($19.5\ k_BT$) and heptylglucoside ($18.0\ k_BT$), suggesting comparably high spontaneous curvature of cholate containing aggregates.

picture of micelle-to-vesicle transformation. The latter is dominated and controlled by the final mixed aggregate composition. It thus produces similar final results so long as the rate of relative composition change remains the same. In contrast, the surfactant-induced vesicle solubilisation typically creates a plethora of intermediate structures. Some are long-lived and differ in size despite their similar composition. Kinetic trapping is an additional, and relatively more likely, problem encountered during vesicle solubilisation studies.

Appendix A. The dissociation constant shift

The primary reason for different molecular dissociation in an aqueous bulk and at a lipid bilayer–water interface is the local dielectric constant variability. Relative permittivity of an aqueous buffer is typically between 70 and 80. Lipid bilayer core has a dielectric constant around 2.5. Lipid bilayer–water interface is somewhere in between (for a phosphatidylcholine–water interface the dielectric constant value normally changes between 20 and 40 over a distance of ~0.5 nm [77]).

The secondary effect underlying apparent dissociation constant shift is the modification of the local proton concentration by H^+ attraction toward a negatively charged surface or repulsion from a positively charged surface. Cholate binding to a bilayer introduces negative charges onto the latter. The resulting local pH shift effectively increases interfacial acidity, due to the Coulomb attraction between the positive protons and the negative surface. The Gouy–Chapman approximation [77,78] is useful for estimating the shift, as it provides the electrostatic surface potential value, ψ, as a function of bilayer bound cholate molecule fraction, interfacial dielectric constant, and bulk salt concentration. From the calculated interfacial electrostatic potential value one can derive the pH shift originating from the Coulomb interactions: $\Delta pH = \log[\exp(-e_0\psi/k_BT)] = -e_0\psi/2.3k_BT$, where e_0 is the elementary electric charge (1.602×10^{-19} C), k_B the Boltzmann constant (1.38×10^{-23} JK^{-1}), and T the absolute temperature. If the mole fraction of the negative molecules in a planar bilayer is $x_e = 0.175$, for example, the difference amounts to $\Delta pH \approx -1$; for molar fraction $x_e = 0.521$ the difference is $\Delta pH \approx -2$ (both at 25 °C, for bulk ionic strength = 150 mM, and neglecting the non-Coulombic contributions).

pH at a membrane surface should therefore exceed $pK_a^{mem} + 2$ to ensure complete (>99%) ionisation of bound cholate molecules. An even safer choice is $pH = pK_a^{mem} + 3$. This corresponds to a bulk pH exceeding $pK_a^{mem} - \Delta pH + 2$ (or 3).

Appendix B. Dependence of the effective bilayer rigidity on the average vesicle size

To account for the dependence of apparent vesicle size changes upon addition of low cholate concentration (region A) on initial vesicle size (Figs. 2–4) we used the mathematical approach derived by Helfrich [40]. This describes the dependency of effective bilayer rigidity on average vesicle size and allows calculation of the softening-induced vesicle size diminution.

Let us write the effective mole fraction of bilayer associated cholate as:

$$x_e = \frac{C_b}{C_b + L} \tag{B1}$$

and the mole fraction of free cholate in the bulk aqueous solution as:

$$x_w = \frac{C_w}{C_w + W} \approx \frac{C_w}{W}, \tag{B2}$$

where C_b is the bound and C_w the bulk cholate concentration. L is the molar lipid and $W \approx 55.5$ M the molar water concentration. The commonly used definition of the apparent cholate partition coefficient between water and lipid bilayer is:

$$P = \frac{x_e}{x_w}. \tag{B3}$$

It should be replaced, in the simplest approximation, with an expression that allows for the Coulomb interaction:

$$P_0 = \frac{x_e}{x_w \cdot \exp[-\varphi]}, \tag{B4}$$

where φ is the bilayer surface dimensionless electrostatic potential. Eq. (B4) conveniently accounts for the Coulomb interactions between the charged cholate molecules in solution and the charges at bilayer surface through the electrostatic Boltzmann factor in the denominator. φ is related to the surface electrostatic potential, ψ, through the relation $\varphi = ze_0\psi/k_BT$. In turn, the electrostatic surface potential depends on cholate concentration at the bilayer surface (for further details see [45,77,78]). For the sake of simplicity, we did not separate the effect of the Coulomb interactions on cholate partition coefficient and true bending rigidity of bilayers. We rather used their apparent values, as follows. Based on the published and on our own unpublished data we estimated the intrinsic "partition coefficient" of cholate in SPC lipid bilayers to be around 1.5×10^4. From this value we calculated the apparent cholate partition coefficient as a function of lipid and total cholate concentration, allowing for the Coulomb electrostatic effects [45,77,78].

By combining Eqs. (B1)–(B3) and considering the relationship $C_{Tot} = C_b + C_w$ we then got:

$$P \approx \frac{C_b W}{(C_b + L)C_w} \approx \frac{C_b W}{(C_b + L)(C_{Tot} - C_b)}. \tag{B5}$$

We calculated C_b as a function of total cholate concentration by numerically solving Eq. (B5) and then derived x_e from Eq. (B1).

To assess the cholate concentration effect on the average vesicle size we first expressed the total (outer + inner) surface area of a spherical bilayer vesicle as:

$$A_v = 4\pi r_v^2 + 4\pi(r_v - d_{mem})^2, \tag{B6}$$

r_v being the vesicle radius and d_{mem} the bilayer thickness (which we took to be 4 nm, as is appropriate for a typical fluid-phase phospholipid). From the starting vesicle area, $A_{v,0}$ (i.e. A_v at $x_e = 0$) we obtained the average number of lipid molecules in each vesicle

$$N_L = \frac{A_{v,0}}{A_L} \tag{B7}$$

in terms of the average area per lipid molecule in a bilayer, A_L, which we took to be 0.65 nm^2. The number of cholate molecules in each mixed bilayer vesicle is then:

$$N_C(x_e) = \frac{x_e}{1 - x_e} N_L. \tag{B8}$$

A_C is the average area of a cholate molecule in the mixed bilayer ($A_C \approx 0.40$ nm^2). The total (outer + inner) surface area of a mixed bilayer vesicle is correspondingly:

$$A_v(x_e) = \left[1 + \frac{x_e}{(1 - x_e)}\frac{A_C}{A_L}\right] A_{v,0}. \tag{B9}$$

Calculation of a mixed, spherical vesicle diameter, or radius, as a function of bilayer associated cholate concentration can be done by numerically solving Eq. (B9) after inserting $A_{v,0}$ and $A_v(x_e)$ from Eq. (B6).

We finally refined the apparent mixed bilayer vesicle size calculation by using the mathematical approach introduced by Helfrich [40]. We accordingly took the difference between the intrinsic and the apparent outer surface of a bilayer vesicle to be:

$$A_{v,\,outer} - A_{v,\,outer,\,app} = r_v^2 \frac{k_B T}{2\kappa} \ln M. \tag{B10}$$

k_B is the Boltzmann constant (1.38×10^{-23} JK^{-1}), T the absolute temperature, and κ the intrinsic, "true" mixed bilayer bending rigidity (which is a function of the cholate concentration in the bilayer).

In the spirit of the Helfrich model we identified the total number of modes on a vesicle with $M = N_C/2 + N_L$, thus clarifying that this quantity depends on cholate concentration in the bilayer as well. By rewriting Eq. (B10) in terms of the vesicle radius we obtained:

$$r_v^2 - r_{v,\,eff}^2 = r_v^2 \frac{k_B T}{8\pi\kappa} \ln M, \tag{B11}$$

$$r_{v,\,eff} = r_v \left[1 - \frac{k_B T}{8\pi\kappa} \ln M\right]^{0.5}. \tag{B12}$$

We combined Eqs. (B5), (B9), and (B12) to analyse the dynamic light scattering data. For this purpose, we programmed a Mathcad calculation sheet (Mathcad version 11.0b, Mathsoft Engineering & Education, Inc., Cambridge, MA, USA). We show the results in Table 2 and Fig. 6.

To analyse the static light scattering data with the same mathematical approach one must consider that the intensity of the light scattered by an aggregate particle is a power-function of the average (presumably spherical) aggregate radius [79,80]. We calculated the corresponding exponent within the framework of the Rayleigh–Gans–Debye approximation for the hollow sphere model [80] to be 3.00–3.33 for the vesicles with the average radius in the range 60–50 nm.

Appendix C. The small mixed micelle composition at the total cholate concentration that ensures complete lipid solubilisation

We used the mathematical model developed by Roth et al. [76] to determine the molecular composition of the mixed aggregates comprised of the solubilised phospholipid and cholate molecules. The model accounts for the finite size of the thread-like micelles and also considers the inhomogeneous cholate distribution between the central micelle part and the end-caps. The total surfactant concentration

$$C_{Tot} = C_w + \left[\frac{L_M}{L} R_e^{sol} + \left(1 - \frac{L_M}{L}\right) R_e^{sat}\right] L - \frac{A_w}{\alpha^{0.5} L^{0.5}} \tag{C1}$$

is a function of the bulk surfactant concentration, C_w, the total lipid concentration, L, and the solubilised (i.e. micellar) lipid concentration, L_M. R_e^{sat} defines the maximum achievable surfactant molar ratio in a vesicle bilayer (i.e. the saturation limit) and R_e^{sol} the surfactant molar ratio ensuring complete lipid solubilisation into mixed micelles within the framework of the three-stage solubilisation model. The effective surfactant molar ratio in an aggregate is generally given by: $R_e = C_b/L$, where C_b is the lipid-associated (i.e. bound) surfactant concentration.

A_w is an adjustable parameter that takes into account the scission energy [76]. Scission of a thread-like micelle is a physical process resulting in creation of two end-caps. To create an end-cap from the cylindrical part of a micelle an energy ϵ is required; the energy 2ϵ is thus called the scission energy [81]. According to Kozlov et al. [82] and Roth et al.[76], the scission energy should be qualitatively smaller for a surfactant with a higher spontaneous curvature, which typically corresponds to shorter hydrocarbon chains. For a surfactant requiring lower scission energy the phase boundaries should deviate from the straight line over a broader concentration range, beginning already at high lipid concentrations and extending toward the low concentration end [76].

An alternative form of Eq. (C1), written in terms of the relative lipid concentration in micelles, $\alpha = L_M/L$, is:

$$C_{Tot} = C_w + \left[\alpha R_e^{sol} + (1-\alpha) R_e^{sat}\right] L - \frac{A_w}{\alpha^{0.5} L^{0.5}}. \tag{C2}$$

Eq. (C2) is useful for fitting data measured with aggregates of *known and constant* composition. Our turbidimetric measurements can quantitatively and reliably reveal only the effective surfactant molar ratio in the small micellar aggregates, R_e^{sol}, for which $\alpha = 1$, and thus:

$$C_{Tot} = C_w + R_e^{sol} L - \frac{A_w}{L^{1/2}}. \tag{C3}$$

The negatively charged cholate molecules in mixed amphipat aggregates affect the surfactant distribution between micelles/vesicle bilayers and bulk solution. To assess more properly the association (expressed here for the sake of convenience as partition coefficient) of cholate in the tested aggregates we included the Coulomb interactions into our data analysis (but neglected for the sake of simplicity all the non-Coulomb effects). To this effect, we expressed the surface charge density

$$\sigma(R_e) = z e_0 \frac{R_e}{A_L + R_e A_C} \tag{C4}$$

as a function of the aggregate bound, charged surfactant valence, $z = 1$, the molar ratio of the charged surfactant in the aggregate, R_e, the elementary electric charge, $e_0 = 1.602\times10^{-19}$ C, the area per surfactant molecule in the mixed aggregates, A_C, and the area per lipid molecule in the mixed aggregate, A_L.

Another important system descriptor is the Debye screening length, λ_D, which describes the electrostatic interaction reach. For a symmetric monovalent (i.e. 1:1) electrolyte solution with the bulk salt concentration C_{el} one can express the Debye length as:

$$\lambda_D = \sqrt{\frac{\varepsilon_0 \varepsilon_r k_B T}{2000 e_0^2 N_A C_{el}}}. \tag{C5}$$

ε_0 is the permittivity of free space (8.8542×10^{-12} As/Vm), ε_r the relative permittivity (i.e. the dielectric constant) of the bulk solution, k_B the Boltzmann constant, T the absolute temperature, and N_A the Avogadro's number (6.02205×10^{23} mol^{-1}).

For a spherical surface, which we use herein as the simplest possible proxy for the small mixed micelles, in a 1:1 electrolyte, the relationship between the electrostatic potential and the surface charge density is [83]:

$$\sigma = \frac{\varepsilon_0 \varepsilon_b k_B T}{\lambda_D e_0} \cdot 2 \sinh\left(\frac{\varphi}{2}\right) \cdot \left[1 + \frac{2\lambda_D}{r_v \cosh^2\left(\frac{\varphi}{4}\right)} + \frac{8\lambda_D^2 \ln\left(\cosh\left(\frac{\varphi}{4}\right)\right)}{r_v^2 \sinh^2\left(\frac{\varphi}{2}\right)}\right]^{0.5}. \tag{C6}$$

ε_b is the local dielectric constant near the surface associated charges and φ the normalised dimensionless electrostatic potential at the micellar surface. We used Eq. (C6) to calculate φ and then the surface electrostatic potential, $\psi = \varphi k_B T/z e_0$, from the surface charge density, σ (for the much larger, and thus quasi-planar, bilayer vesicle surface one would have to use the corresponding Gouy–Chapman expression for a planar surface instead of Eq. (C6)). The effective mole fraction of cholate in the mixed aggregates, x_e, the cholate mole fraction in the bulk solution, x_w, and the cholate partition coefficient in the mixed micelles is then derivable from Eqs. (B1), (B2), and (B4), respectively.

Appendix D

Our experimental data suggest that the structural conversions observed with the mixed phosphatidylcholine–cholate aggregates could involve two bicontinuous, parallel aggregate size changes. To corroborate the plausibility of such notion, and to mimic the measured optical density *vs.* total cholate concentration curves, we combined two sigmoidal functions, each with the following basic mathematical form:

$$f(x, x_0, S) = \frac{1}{1 + \exp[S(x - x_0)]}. \quad \text{(D1)}$$

We assumed the first sigmoidal function to be centred around x_0 and to have the width described by S. We postulated the second sigmoidal curve to have a width different by dS and to be shifted relative to the first curve by dx_0, i.e. we assumed the second curve centre to be at $x_0 + dx_0$ and the second curve width to be $S + dS$. We moreover postulated the second sigmoidal function to differ from the first one in height by a factor of n, by writing:

$$f_{1+2}(x, x_0, S, dx_0, dS, n) = f(x, x_0, S) - n \cdot f(x, x_0 + dx_0, S + dS) \quad \text{(D2)}$$

We then assigned different *ad hoc* values to each adjustable parameter of such *purely phenomenological* model. Certain tested parameter combinations simulated qualitatively each curve form those found in our static light scattering data, as is illustrated in Fig. 9.

We do not doubt that we could achieve an even closer match by optimising the adjustable parameter values. This proves to us that a simple combination of two parallel processes—one increasing and one decreasing the average aggregate size—can explain the main features of the cholate-induced vesicle transformation into small mixed amphipat micelles. To elucidate the finer features, such as tailing, further and/or more complicated processes need to be invoked.

References

[1] P. Garidel, A. Hildebrand, K. Knauf, A. Blume, Membranolytic activity of bile salts: influence of biological membrane properties and composition, Molecules 12 (2007) 2292–2326.
[2] R. Schubert, Relationship between the structure of bile salts and their interaction with membrane lipids, Proceedings of M.o.B.B.E.L., vol. 4, Tannheim, Austria, 1989, pp. 1–17.
[3] A. Helenius, K. Simons, Solubilization of membranes by detergents, Biochim. Biophys. Acta 415 (1975) 29–79.
[4] M. Ollivon, S. Lesieur, C. Grabielle-Madelmont, M. Paternostre, Vesicle reconstitution from lipid–detergent mixed micelles, Biochim. Biophys. Acta 1508 (2000) 34–50.
[5] M.-T. Paternostre, M. Roux, J.-L. Rigaud, Mechanisms of membrane protein insertion into liposomes during reconstitution procedures involving the use of detergents. 1. Solubilization of large unilamellar liposomes (prepared by reverse-phase evaporation) by Triton X-100, octyl glucoside, and sodium cholate, Biochemistry 27 (1988) 2668–2677.
[6] J.-L. Rigaud, B. Pitard, D. Levy, Reconstitution of membrane proteins into liposomes: application to energy-transducing membrane proteins, Biochim. Biophys. Acta 1231 (1995) 223–246.
[7] P. Garidel, J. Lasch, Mixed vesicles and mixed micelles: formation, thermodynamic stability, and pharmaceutical aspects, in: G. Gregoriadis (Ed.), Liposome technology, Volume I: Liposome preparation and related techniques, Informa Healthcare USA, Inc., New York, 2007, pp. 209–239.
[8] G. Cevc, Lipid vesicles and other colloids as drug carriers on the skin, Adv. Drug Deliv. Rev. 56 (2004) 675–711.
[9] M.M.A. Elsayed, O.Y. Abdallah, V.F. Naggar, N.M. Khalafallah, Lipid vesicles for skin delivery of drugs: reviewing three decades of research, Int. J. Pharm. 332 (2007) 1–16.
[10] J. Guo, Q. Ping, L. Zhang, Transdermal delivery of insulin in mice by using lecithin vesicles as a carrier, Drug Deliv. 7 (2000) 113–116.
[11] G. Cevc, Transfersomes, liposomes and other lipid suspensions on the skin: permeation enhancement, vesicle penetration, and transdermal drug delivery, Crit. Rev. Ther. Drug Carrier Syst. 13 (1996) 257–388.
[12] G. Cevc, Transdermal drug delivery of insulin with ultradeformable carriers, Clin. Pharmacokinet. 42 (2003) 461–474.
[13] G. Cevc, D. Gebauer, J. Stieber, A. Schätzlein, G. Blume, Ultraflexible vesicles, transfersomes, have an extremely low pore penetration resistance and transport therapeutic amounts of insulin across the intact mammalian skin, Biochim. Biophys. Acta 1368 (1998) 201–215.
[14] M.M.A. Elsayed, O.Y. Abdallah, V.F. Naggar, N.M. Khalafallah, Deformable liposomes and ethosomes as carriers for skin delivery of ketotifen, Pharmazie 62 (2007) 133–137.
[15] A. Paul, G. Cevc, Noninvasive administration of protein antigens: transdermal immunization with bovine serum albumin in transfersomes, Vaccine Res. 4 (1995) 145–164.
[16] A. Paul, G. Cevc, B.K. Bachhawat, Transdermal immunisation with an integral membrane component, gap junction protein, by means of ultradeformable drug carriers, transfersomes, Vaccine 16 (1998) 188–195.
[17] S. Almog, T. Kushnir, S. Nir, D. Lichtenberg, Kinetic and structural aspects of reconstitution of phosphatidylcholine vesicles by dilution of phosphatidylcholine–sodium cholate mixed micelles, Biochemistry 25 (1986) 2597–2605.
[18] A. De la Maza, J.L. Parra, Vesicle to micelle phase transitions involved in the interaction of sodium cholate with phosphatidylcholine liposomes, Colloids Surf. A 127 (1997) 125–134.
[19] A. Hildebrand, R. Neubert, P. Garidel, A. Blume, Bile salt induced solubilization of synthetic phosphatidylcholine vesicles studied by isothermal titration calorimetry, Langmuir 18 (2002) 2836–2847.
[20] M.A. Long, E.W. Kaler, S.P. Lee, Structural characterization of the micelle–vesicle transition in lecithin–bile salt solutions, Biophys. J. 67 (1994) 1733–1742.
[21] D. Meyuhas, A. Bor, I. Pinchuk, A. Kaplun, Y. Talmon, M.M. Kozlov, D. Lichtenberg, Effect of ionic strength on the self-assembly in mixtures of phosphatidylcholine and sodium cholate, J. Colloid Interface Sci. 188 (1997) 351–362.
[22] R. Schubert, K.H. Schmidt, Structural changes in vesicle membranes and mixed micelles of various lipid compositions after binding of different bile salts, Biochemistry 27 (1988) 8787–8794.
[23] D.M. Small, A classification of biologic lipids based upon their interaction in aqeous systems, J. Am. Oil Chem. Soc. 45 (1968) 108–119.
[24] A. Walter, P.K. Vinson, A. Kaplun, Y. Talmon, Intermediate structures in the cholate–phosphatidylcholine vesicle–micelle transition, Biophys. J. 60 (1991) 1315–1325.
[25] J.S. Pedersen, S.U. Egelhaaf, P. Schurtenberger, Formation of polymerlike mixed micelles and vesicles in lecithin–bile salt solutions: a small-angle neutron-scattering study, J. Phys. Chem. 99 (1995) 1299–1305.
[26] R.P. Hjelm Jr., P. Thiyagarajan, H. Alkan-Onyuksel, Organization of phosphatidylcholine and bile salt in rodlike mixed micelles, J. Phys. Chem. 96 (1992) 8653–8661.
[27] N.A. Mazer, G.B. Benedek, M.C. Carey, Quasielastic light-scattering studies of aqueous biliary lipid systems. Mixed micelle formation in bile salt–lecithin solutions, Biochemistry 19 (1980) 601–615.
[28] M.C. Carey, D.M. Small, Micelle formation by bile salts. Physical–chemical and thermodynamic considerations, Arch. Intern. Med. 130 (1972) 506–527.
[29] A. Alonso, R. Sáez, A. Villena, F.M. Goñi, Increase in size of sonicated phospholipid vesicles in the presence of detergents, J. Membr. Biol. 67 (1982) 55–62.
[30] W. Shankland, The equilibrium and structure of lecithin–cholate mixed micelles, Chem. Phys. Lipids 4 (1970) 109–130.
[31] D.M. Small, M.C. Bourgès, D.G. Dervichian, The biophysics of lipidic associations: I. The ternary systems lecithin–bile salt–water, Biochim. Biophys. Acta 125 (1966) 563–580.
[32] A. Nasner, L. Kraus, Quantitative Bestimmung von Phosphatidylcholin mit Hilfe der HPLC, Fette, Seifen, Anstrichmittel 83 (1981) 70–73.
[33] M. Grit, D.J.A. Crommelin, J. Lang, Determination of phosphatidylcholine, phosphatidylglycerol and their lyso forms from liposome dispersions by high-performance liquid chromatography using high-sensitivity refractive index detection, J. Chromatogr. 585 (1991) 239–246.
[34] S.W. Provencher, CONTIN: a general purpose constrained regularization program for inverting noisy linear algebraic and integral equations, Comput. Phys. Commun. 27 (1982) 229–242.
[35] S.W. Provencher, A constrained regularization method for inverting data represented by linear algebraic or integral equations, Comput. Phys. Commun. 27 (1982) 213–227.
[36] G. Pereira, R. Moreira, M.J. Vázquez, F. Chenlo, Kinematic viscosity prediction for aqueous solutions with various solutes, Chem. Eng. J. 81 (2001) 35–40.
[37] T. Wang, T.-C. Bai, W. Wang, J.-J. Zhu, C.-W. Zhu, Viscosity and activation parameters of viscous flow of sodium cholate aqueous solution, J. Mol. Liq. 142 (2008) 150–154.
[38] H. Schmiedel, L. Almásy, G. Klose, Multilamellarity, structure and hydration of extruded POPC vesicles by SANS, Eur. Biophys. J. 35 (2006) 181–189.
[39] M.J. Hope, M.B. Bally, G. Webbb, P.R. Cullis, Production of large unilamellar vesicles by a rapid extrusion procedure. Characterization of size distribution, trapped volume and ability to maintain a membrane potential, Biochim. Biophys. Acta 812 (1985) 55–65.
[40] W. Helfrich, Size distributions of vesicles: the role of the effective rigidity of membranes, J. Physique 47 (1986) 321–329.
[41] J.F. Faucon, M.D. Mitov, P. Méléard, I. Bivas, P. Bothorel, Bending elasticity and thermal fluctuations of lipid membranes. Theoretical and experimental requirements, J. Physique 50 (1989) 2389–2414.
[42] H.I. Petrache, N. Gouliaev, S. Tristram-Nagle, R. Zhang, R.M. Suter, J.F. Nagle, Interbilayer interactions from high-resolution X-ray scattering, Phys. Rev. E 57 (1998) 7014–7024.
[43] W. Rawicz, K.C. Olbrich, T. McIntosh, D. Needham, E. Evans, Effect of chain length and unsaturation on elasticity of lipid bilayers, Biophys. J. 79 (2000) 328–339.
[44] T. Nakashima, T. Anno, H. Kanda, Y. Sato, T. Kuroi, H. Fujii, S. Nagadome, G. Sugihara, Potentiometric study on critical micellization concentrations (CMC) of

sodium salts of bile acids and their amino acid derivatives, Colloids Surf. B: Biointerfaces 24 (2002) 103–110.
[45] M.M. Elsayed, U. Vierl, G. Cevc, Accurate potentiometric determination of lipid membrane–water partition coefficients and apparent dissociation constants of ionizable drugs: electrostatic corrections, Pharm. Res. 26 (2009) 1332–1343.
[46] D.J. Cabral, J.A. Hamilton, D.M. Small, The ionization behavior of bile acids in different aqueous environments, J. Lipid. Res. 27 (1986) 334–343.
[47] D.M. Small, D.J. Cabral, D.P. Cistola, J.S. Parks, J.A. Hamilton, The ionization behavior of fatty acids and bile acids in micelles and membranes, Hepatology 4 (1984) 77S–79S.
[48] M. Grit, D.J. Crommelin, The effect of surface charge on the hydrolysis kinetics of partially hydrogenated egg phosphatidylcholine and egg phosphatidylglycerol in aqueous liposome dispersions, Biochim. Biophys. Acta 1167 (1993) 49–55.
[49] M. Grit, J.H. de Smidt, A. Struijke, D.J. Crommelin, Hydrolysis of phosphatidylcholine in aqueous liposome dispersions, Int. J. Pharm. 50 (1989) 1–6.
[50] A. Hildebrand, K. Beyer, R. Neubert, P. Garidel, A. Blume, Temperature dependence of the interaction of cholate and deoxycholate with fluid model membranes and their solubilization into mixed micelles, Colloids Surf. B: Biointerfaces 32 (2003) 335–351.
[51] F. Ollila, J.P. Slotte, A thermodynamic study of bile salt interactions with phosphatidylcholine and sphingomyelin unilamellar vesicles, Langmuir 17 (2001) 2835–2840.
[52] J. Leng, S.U. Egelhaaf, M.E. Cates, Kinetic pathway of spontaneous vesicle formation, Europhys. Lett. 59 (2002) 311–317.
[53] S.U. Egelhaaf, P. Schurtenberger, Micelle-to-vesicle transition: a time-resolved structural study, Phys. Rev. Lett. 82 (1999) 2804–2807.
[54] S.U. Egelhaaf, U. Olsson, P. Schurtenberger, Time-resolved SANS for surfactant phase transitions, Physica B 276–278 (2000) 326–329.
[55] J. Leng, S.U. Egelhaaf, M.E. Catesa, Kinetics of the micelle-to-vesicle transition: aqueous lecithin–bile salt mixtures, Biophys. J. 85 (2003) 1624–1646.
[56] H. Heerklotz, Interactions of surfactants with lipid membranes, Q. Rev. Biophys. 41 (2008) 205–264.
[57] C. Sun, Y. Sano, H. Kashiwagi, M. Ueno, Characterization of aggregate structures of phospholipid in the process of vesicle solubilization with sodium cholate using laser light scattering method, Coll. Polym. Sci. 280 (2002) 900–907.
[58] P.K. Vinson, Y. Talmon, A. Walter, Vesicle–micelle transition of phosphatidylcholine and octyl glucoside elucidated by cryo-transmission electron microscopy, Biophys. J. 56 (1989) 669–681.
[59] E. Evans, W. Rawicz, A.F. Hoffman, Lipid bilayer expansion and mechanical disruption in solution of water–soluble bile acid, in: A.F. Hoffman, G. Paumgartner, A. Stiehl (Eds.), Bile Acids in Gastroenterology: Basic and Clinical Advances: Proceedings of the 80th Falk Symposium, Kluwer Academic Publishers, Lancaster, 1995, pp. 59–68.
[60] G. Cevc, A.G. Schätzlein, H. Richardsen, U. Vierl, Overcoming semipermeable barriers, such as the skin, with ultradeformable mixed lipid vesicles, transfersomes, liposomes, or mixed lipid micelles, Langmuir 19 (2003) 10753–10763.
[61] G. Cevc, G. Blume, A. Schätzlein, D. Gebauer, A. Paul, The skin: a pathway for systemic treatment with patches and lipid-based agent carriers, Adv. Drug Deliv. Rev. 18 (1996) 349–378.
[62] G. Cevc, D. Gebauer, Hydration-driven transport of deformable lipid vesicles through fine pores and the skin barrier, Biophys. J. 84 (2003) 1010–1024.
[63] F. Nomura, M. Nagata, T. Inaba, H. Hiramatsu, H. Hotani, K. Takiguchi, Capabilities of liposomes for topological transformation, Proc. Natl. Acad. Sci. U. S. A. 98 (2001) 2340–2345.
[64] M.F. Brown, R.L. Thurmond, S.W. Dodd, D. Otten, K. Beyer, Elastic deformation of membrane bilayers probed by deuterium NMR relaxation, J. Am. Chem. Soc. 124 (2002) 8471–8484.
[65] S. Leibler, Curvature instability in membranes, J. Physique 47 (1986) 507–516.
[66] C. Wachter, U. Vierl, G. Cevc, Adaptability and elasticity of the mixed lipid bilayer vesicles containing non-ionic surfactant designed for targeted drug delivery across the skin, J. Drug Target. 16 (2008) 611–625.
[67] D.J. Cabral, D.M. Small, H.S. Lilly, J.A. Hamilton, Transbilayer movement of bile acids in model membranes, Biochemistry 26 (1987) 1801–1804.
[68] J.M. Donovan, A.A. Jackson, Transbilayer movement of fully ionized taurine-conjugated bile salts depends upon bile salt concentration, hydrophobicity, and membrane cholesterol content, Biochemistry 36 (1997) 11444–11451.
[69] M. Ueno, N. Hirota, H. Kashiwagi, S. Sagasaki, Process of destruction of large unilamellar vesicles by a nonionic detergent, octylglucoside, and size growth factor in vesicle formation from phospholipid–detergent mixed micelles, Coll. Polym. Sci. 282 (2003) 69–75.
[70] P. Fromherz, Modulation of the edge-tension of lipid membranes by cholate and cholesterol and the micelle–vesicle transition in model bile systems, in: W. Swobodnik, H. Ditschuneit, R.D. Soloway (Eds.), Gallstone Disease, Springer, Berlin, 1990, pp. 27–33.
[71] P. Fromherz, Lipid–vesicle structure: size control by edge-active agents, Chem. Phys. Lett. 94 (1983) 259–266.
[72] P. Schurtenberger, N. Mazer, S. Waldvogel, W. Känzig, Preparation of monodisperse vesicles with variable size by dilution of mixed micellar solutions of bile salt and phosphatidylcholine, Biochim. Biophys. Acta 775 (1984) 111–114.
[73] D.D. Lasič, A molecular model for vesicle formation, Biochim. Biophys. Acta 692 (1982) 501–502.
[74] R. Schubert, Liposome preparation by detergent removal, Methods Enzymol. 367 (2003) 46–70.
[75] H.G. Weder, O. Zumbuehl, The preparation of variably sized homogenous liposomes for laboratory, clinical, and industrial use by controlled detergent dialysis, in: G. Gregoriadis (Ed.), Liposome Technology, Volume I: Preparation of Liposomes, CRC press, Boca Raton, 1984, pp. 79–107.
[76] Y. Roth, E. Opatowski, D. Lichtenberg, M.M. Kozlov, Phase behavior of dilute aqueous solutions of lipid–surfactant mixtures: effects of finite size of micelles, Langmuir 16 (2000) 2052–2061.
[77] G. Cevc, Membrane electrostatics, Biochim. Biophys. Acta 1031 (1990) 311–382.
[78] G. Cevc, Electrostatic characterization of liposomes, Chem. Phys. Lipids 64 (1993) 163–186.
[79] C.S. Chong, K. Colbow, Light scattering and turbidity measurements on lipid vesicles, Biochim. Biophys. Acta 436 (1976) 260–282.
[80] M.M.A. Elsayed, G. Cevc, Turbidity spectroscopy as a means for accurate size characterization of submicroscopic, nanosized drug carriers, such as nanoparticles and lipid vesicles, (2010) In preparation.
[81] M.E. Cates, S.J. Candau, Statics and dynamics of worm-like surfactant micelles, J. Phys. Condens. Matter. 2 (1990) 6869–6892.
[82] M.M. Kozlov, D. Lichtenberg, D. Andelman, Shape of phospholipid/surfactant mixed micelles: cylinders or disks? Theoretical analysis, J. Phys. Chem. B 101 (1997) 6600–6606.
[83] H. Ohshima, T.W. Healy, L.R. White, Accurate analytic expressions for the surface charge density/surface potential relationship and double-layer potential distribution for a spherical colloidal particle, J. Colloid Interface Sci. 90 (1982) 17–26.